Microsc. Microanal. 20, 1638–1645, 2014
doi:10.1017/S1431927614013476

Microscopy AND Microanalysis

Convenient Preparation of High-Quality Specimens for Annealing Experiments in the Transmission Electron Microscope

Martial Duchamp,[1,*] Qiang Xu,[2,3] and Rafal E Dunin-Borkowski[1]

[1]*Ernst Ruska-Center for Microscopy and Spectroscopy with Electrons (ER-C) and Peter Grünberg Institute, Forschungszentrum Jülich, 52428 Jülich, Germany*
[2]*DENSsolutions, 2628XH Delft, The Netherlands*
[3]*Kavli Institute of Nanoscience, Delft University of Technology, 2628CJ Delft, The Netherlands*

Abstract: A procedure based on focused ion beam milling and *in situ* lift-out is introduced for the preparation of high-quality specimens for *in situ* annealing experiments in the transmission electron microscope. The procedure allows an electron-transparent lamella to be cleaned directly on a heating chip using a low ion energy and back-side milling in order to minimize redeposition and damage. The approach is illustrated through the preparation of an Al–Mn–Fe complex metallic alloy specimen.

Key words: transmission electron microscopy, specimen preparation, focused ion beam milling, *in situ* annealing

Introduction

In situ annealing experiments in the transmission electron microscope (TEM) permit real-time observations of thermally activated processes, such as the evolution of stress in thin films (Venkatraman et al., 1990), recrystallization processes (Zheng et al.,1991), abnormal grain growth (Longworth & Thompson, 1991), interdiffusion (Radulescu et al., 2000), and dislocation propagation (Legros et al., 2001). Until now, most TEM specimens used for *in situ* experiments have been 3-mm-diameter samples prepared by conventional preparation techniques. Such specimen geometries make *in situ* annealing experiments very challenging as a result of the need to heat an entire 3-mm sample, which results in drift owing to thermal expansion of the specimen stage. Although water cooling can be used to mitigate excessive heating of the specimen stage, it is difficult to balance heating power and cooling rate to set an equilibrium temperature. Recent developments in microelectromechanical systems (MEMS)-based heating stages open new opportunities for easy, fast, and reliable *in situ* annealing experiments (van Huis et al., 2008, 2009; Figuerola et al., 2010; Xu et al., 2013). However, approaches for TEM specimen preparation for MEMS devices have not yet been optimized.

Focused ion beam (FIB) milling is a well-established technique for preparing specimens for TEM (Giannuzzi et al., 1997; Langford & Petford-Long, 2000; Kempshall et al., 2002; Rogers et al., 2005; Jeangros et al., 2010; Harlow et al., 2014). The main advantages of FIB milling over conventional TEM specimen preparation include fast and reproducible preparation and site specificity. *In situ* FIB milling and lift-out have been used to prepare micrometer-wide lamellae after deposition of bulk specimens onto straining devices (Field & Papin, 2004). Radulescu et al. (2000) prepared a TEM lamella to study interdiffusion of Pd and Ge contacts to GaAs at temperatures below 400°C. It has also been shown that the implantation of Ga can be reduced by a factor of 2.5–3.0 by reducing the final milling voltage from 30 to 5 kV (Langford et al., 2001). Recently, owing to improvements in ion optics, low energy milling can be used without sacrificing spatial resolution during imaging in the FIB. FIB-prepared specimens have also been shown to be suitable for atomic-resolution spectroscopy (Ramasse et al., 2009) and imaging (Schaffer et al., 2012).

Here, we report on developments in the fabrication of TEM specimens for *in situ* annealing experiments using a MEMS-based heating system. We illustrate the method by presenting results obtained from the Al–Mn–Fe phase of a complex metallic alloy (CMA), for which the understanding of plastic deformation and dislocation mechanisms, both under strain and at elevated temperature, are important (Heggen et al., 2010, 2011; Balanetshyy et al., 2011). The specimen is shown to have few preparation artifacts, crystallographic integrity, and little Ga contamination. More details about *in situ* TEM observations of dislocation propagation at elevated temperature in this alloy will be reported separately.

Materials and Methods

An FEI dual-beam FIB Helios (FEI Company, Eindhoven, The Netherlands) workstation equipped with (1) an *in situ* micro-manipulator, (2) a Pt gas injector system, (3) an α-flip (AF) stage, and (4) a scanning transmission electron microscope (STEM) detector was used for this work. MEMS chips from DENSsolutions (DENSsolutions, Delft, Pays-Bas) were held on the AF stage using a homemade holder, whose

Received April 29, 2014; accepted October 6, 2014
*Corresponding author. martial.duchamp@gmail.com

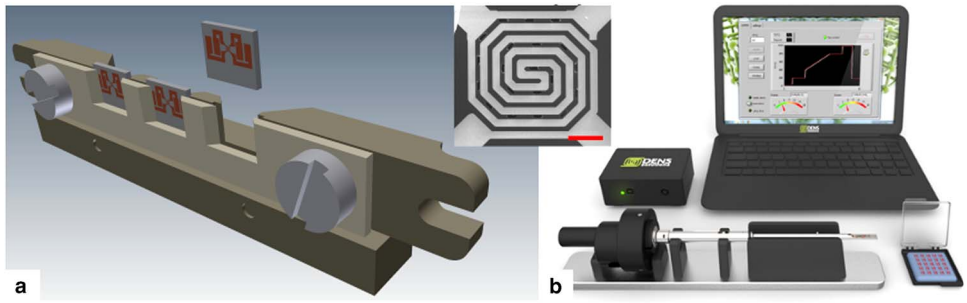

Figure 1. a: Design drawing of a homemade focused ion beam holder used to mount multiple DENSsolutions heater chips onto an FEI Nanolab flip stage. **b:** The main components of the DENSsolutions double-tilt heating system. The inset shows a micro-hotplate at the center of a heater chip with electron-transparent windows. The scale bar is 100 µm.

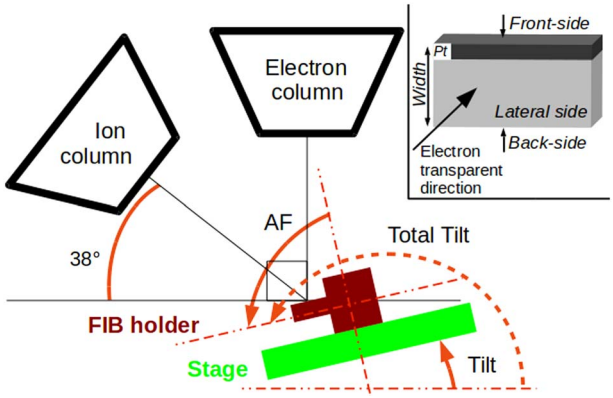

Figure 2. Schematic diagram showing the configuration of an FEI dual-beam FIB Helios workstation with the α-flip (AF) holder mounted on the stage. The solid orange lines show the AF and tilt angles. The dotted orange line shows the total tilt angle of the specimen compared with the horizontal. The inset shows a schematic diagram of a transmission electron microscopic lamella to define the terms used in the text. FIB, focused ion beam.

design is shown in Figure 1. By using this holder, the chips could be tilted from −4 to 60° using the stage tilt and by an additional 0–100° using the AF stage, resulting in a total available tilt range of 164°. The geometry of the FEI workstation and the definition of the angles used in this study are shown in Figure 2. In order to minimize surface damage using low-voltage FIB milling while maintaining good spatial resolution, before starting the procedure the currents and voltages of the ion and electron beams were aligned and set to be coincident. Successful TEM sample preparation with minimal damage was achieved by not irradiating the lamella directly, but by imaging its surfaces only using a "reduced area" that did not coincide with the region of interest. According to the nomenclature used in the FEI software (FEI Company, xT, 2003), the "regular cross-section" (RCS) scanning pattern for milling staircase-shaped patterns was used for almost all of the milling steps, with the exception of steps 4, 5, and 6 (see Table 1), for which FEI's "rectangle" scanning pattern was used for Pt deposition.

TEM experiments were carried out in an FEI Tecnai G20 microscope (FEI Company, Eindhoven, The Netherlands) operated at 200 kV, with energy-dispersive X-ray (EDX) spectroscopy performed using an EDAX Si(Li) detector (EDAX Inc., Mahwah, NJ, USA). EDX linescans were recorded using an acquisition time of 1 s/pixel at 10 eV/channel.

A DENSsolutions DH30 MEMS-based double-tilt heating holder (Fig. 1b) was used for *in situ* annealing experiments. The heating system comprises four main components: (i) a low-drift TEM holder with electrical connections, (ii) a MEMS-based heating chip, (iii) a computer to control the heating system, and (iv) a control box. A software interface is combined with the control box (outside the TEM) to enable communication between the heater chip and the computer. Each heating chip is used as a sample carrier that replaces a traditional TEM grid and has dimensions of 3.9 × 3.2 mm. It contains a micrometer-sized Pt spiral, which is sandwiched inside a nanometer-thick SiN_x membrane that is used as a micro-hotplate and requires only a few milliwatt to heat a sample from room temperature to 1,000°C. Owing to the small mass and thermal capacity of this structure, its temperature can be changed at a rate of 10^5 °C/s, achieving a stability of 10^{-3} °C/s within a few seconds, resulting in minimal specimen drift. It therefore offers a stable platform for atomic-resolution *in situ* heating/biasing experiments. Between the Pt spirals, there are multiple micrometer-sized electron-transparent windows, where a TEM lamella can be placed. These windows can be made of thin amorphous SiN_x, amorphous C, or, for the procedure described in this paper, can be left free in the form of holes.

Results and Discussion

Here, we present results illustrating a FIB-based approach for specimen preparation for *in situ* TEM annealing experiments using heater chips.

Specimen Transfer onto the Heater Chip

This section describes the release and transfer of a thick TEM lamella with dimensions of ~20 × 10 × 3 µm from a bulk specimen onto a heater chip. As TEM specimen preparation is highly material dependent, the milling voltages and currents described here are appropriate for a CMA sample and may need to be adjusted for other materials. This section is divided into three parts: (i) release of a thick TEM lamella from a bulk specimen, (ii) rotation of the lamella on the AF

Table 1. Parameters used during transfer of a 20103 µm lamella from bulk material to a double-tilt heater chip.

Step		Voltage (kV)	Current (nA)	Thickness (µm)	Micro-manipulator	Pt or C Needle	AF Tilt (°)	Specimen Tilt (°)	Total Tilt (°)	Figures
	Release of TEM lamella from bulk material									
1	Deposition of protective Pt layer using e-beam	5	5.5	0.1	Out	In (on)		0	0	
2	Deposition of protective Pt layer using FIB	30	0.28	1	Out	In (on)		52	52	3a
3	Trench milling	30	9.3		Out	Out		52	52	
4	Milling of the lower part	30	6.5		Out	Out		0	0	3b
5	Milling of the lower part after rotation by 180°	30	6.5		Out	Out		0	0	
6	Attachment of micro-manipulator tip	30	0.093		In	In (on)		0	0	3c
7	Release of lamella from bulk material	30	0.093		In	In (off)		0	0	
	Transfer of TEM lamella to the TEM grid									
8	First attachment to TEM grid	5	0.081		In	In (on)	0[a] 90[b]	0	90[a] 180[b]	3d
9	First release of lamella from micro-manipulator	5	0.15		In	In (off)	0[a] 90[b]	0	90[a] 180[b]	3e
10	Rotation to AF tilt of 0°				Out	Out	0[a] 0[b]	0	90[a] 0[b]	3f
11	Attachment of micro-manipulator tip	5	0.081		In	In (on)	90[a] 0[b]	0	180[a] 90[b]	3g
12	Release of lamella from TEM grid	5	0.15		In	In (off)	90[a] 0[b]	0	180[a] 90[b]	
	Transfer of TEM lamella to heater chip									
13	Attachement of lamella to heater chip	5	0.081		In	In (off)	90	13	193	3i
14	Release of lamella from micro-manipulator	5	0.081		In	In (on)	90	13	193	
	Thinning procedure (material dependent)									
15		5	0.45	2[c]	Out	Out	13	47–57	150–160	
16		5	0.15	1.3[c]	Out	Out	13	48–56	151–159	
17		5	0.081	0.5[c]	Out	Out	13	48–56	151–159	
18		5	0.047	0.1[c]	Out	Out	13	47–57	150–160	
19		5	0.028	0.1[d]	Out	Out	13	54–60	157–163	

[a]Parameters for front-side milling.
[b]Parameters for back-side milling.
[c]Milling parameters used down to the given thickness.
[d]Set point for *z* value, using RCS pattern.
AF, *α*-flip; FIB, focused ion beam; TEM, transmission electron microscope; RCS, regular cross-section.
The thicknesses are approximate values measured from FIB images.

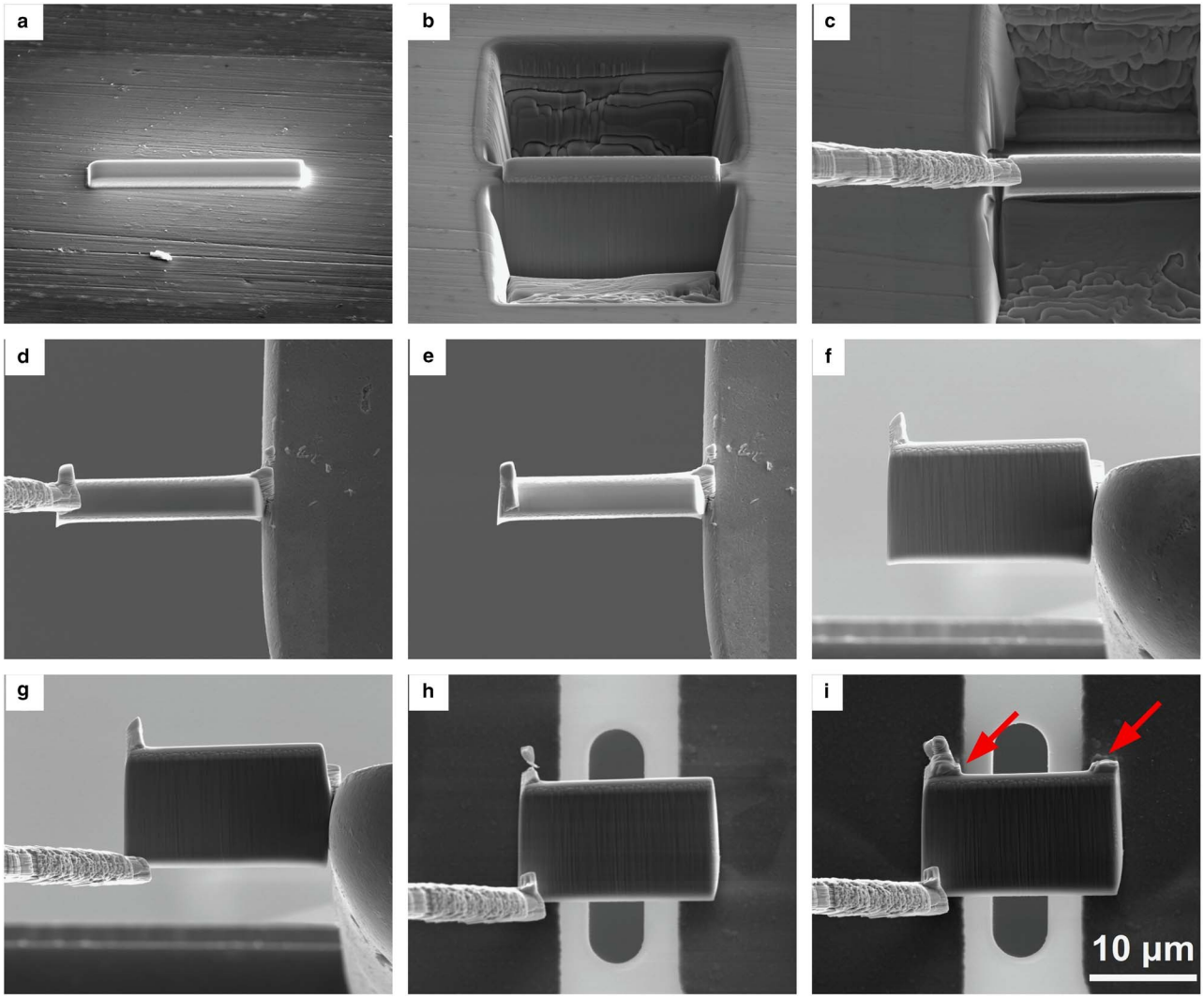

Figure 3. a–i: Scanning electron microscopic images of the different steps used to transfer a 20103 µm lamella from bulk material to a double-tilt heater chip. The tilt angles, positions of the micro-manipulator and Pt needle, and the deposition and etching parameters are given in Table 1. The red arrows in (i) indicate ion-beam-deposited Pt (see text for details).

stage, and (iii) transfer of the lamella to the heater chip. Before introducing the specimen into the FIB system, it is polished to ensure a flat surface that is free of contaminants, which would lead to the presence of particles on the surface of the sample.

Release of the TEM Lamella

In the present study, the release of a TEM lamella from a bulk specimen is similar to the procedure used in most *in situ* FIB lift-out approaches reported previously (Schaffer et al., 2012). The final milling steps can be performed either in "front-side" or in "back-side" milling configuration (Dunin-Borkowski et al., 2005). In the back-side configuration, the specimen is exposed directly to the FIB during the "thinning steps" (steps 15–19 in Table 1) from the reverse side to that used for Pt deposition (steps 1–2 in Table 1). Although it was not essential for the present study, this approach may be used to reduce curtaining effects arising from the presence of Pt nanocrystals in the protection layer and variations in surface composition or roughness. As there is usually no Pt layer on the back side of the specimen, the width of the lamella should be sufficient to retain undamaged regions close to the front side (step 1 in Table 1). Figure 3 shows the key steps in this procedure: (i) deposition of the Pt protection layers, (ii) partial release of the thick lamella, and (iii) its attachment to the micro-manipulator. It is important to perform the "bottom milling" steps using an L-shaped pattern and to rotate the specimen by 180° between steps 4 and 5, as shown in Table 1. In this way, the back side of the lamella takes the form of a V shape and the line on the upper surface of the lamella (marked as a dotted line in Fig. 4a) indicates its center, allowing for optimal positioning of the milling patterns during the "thinning steps" in the back-side milling configuration.

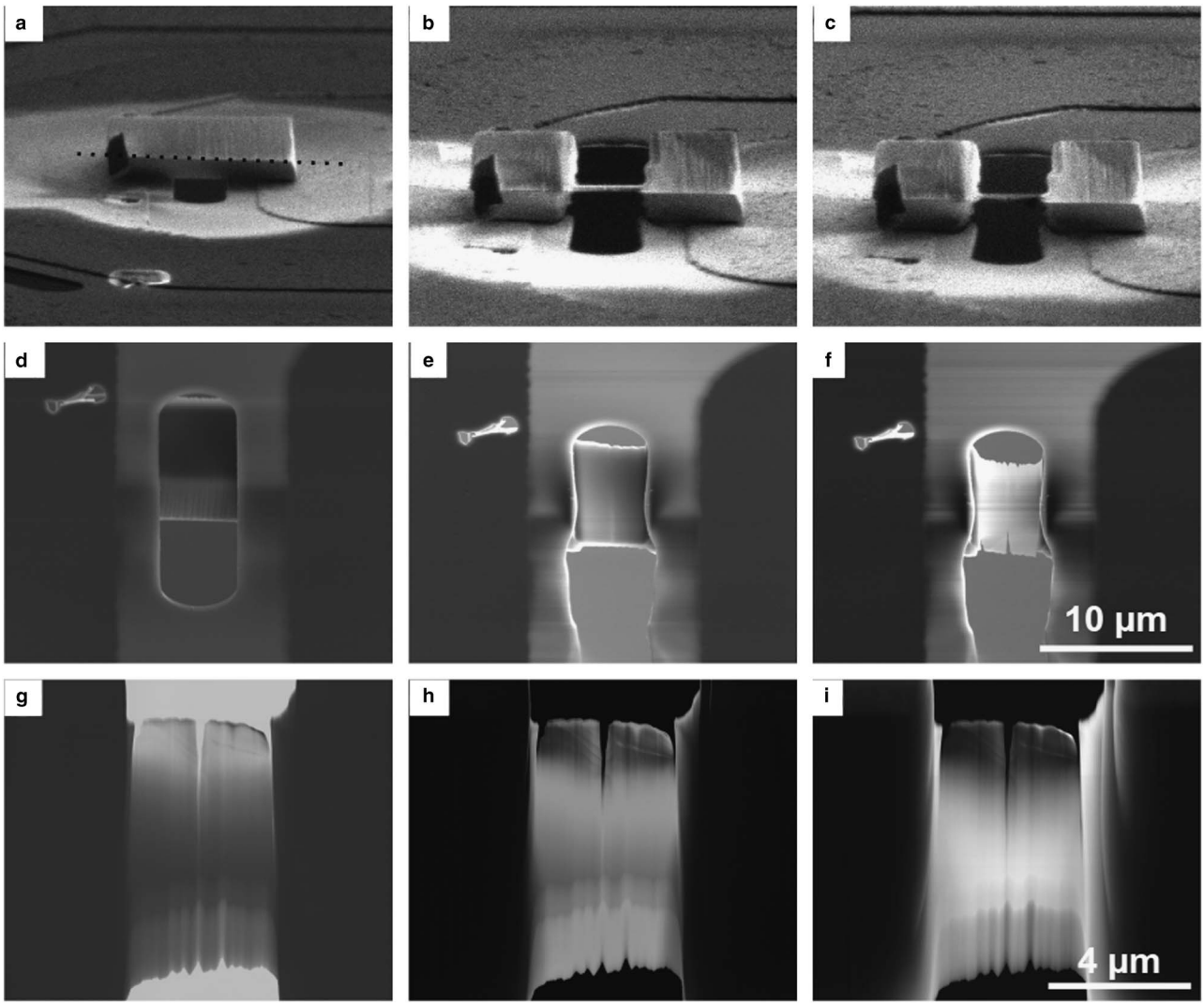

Figure 4. a-c: Focused ion beam (FIB) and (**d–f**) scanning electron microscopic (SEM) images of the different thinning steps. The tilt angles and milling parameters are given in Table 1: (**a**) and (**d**) were acquired after transfer of the lamella onto the chip; (**b**) and (**e**) were acquired after milling at 81 pA (step 17 in Table 1); and (**c**) and (**f**) after milling at 47 pA (step 18 in Table 1); (**g**) bright-field; (**h**) dark-field; and (**i**) high-angle annular dark-field scanning transmission electron microscopic (STEM) images taken with the STEM detector of the FEI dual-beam Nanolab FIB Helios system. The scale bar for the FIB and SEM images is given in (**f**), while the scale bar of the STEM images is given in (**i**). The dot line in (**a**) shows the edge of the V shape created by the milling in steps 4 and 5 in Table 1, in this way the middle of the lamella can be found when using the back-side milling configuration during the thinning procedure.

Transfer of the TEM Lamella onto the TEM Grid

This part of the procedure involves rotating the lamella by 90° about the horizontal axis so that it is horizontal and ultimately close to being parallel to the heater chip surface. Steps 8–12 in Table 1 describe this process. Moreover, depending on the angle of the Cu grid compared to the lamella, front-side and back-side milling configurations can be performed during the later thinning procedure. Care is required when attaching and releasing the lamella using the micro-manipulator, as any pressure applied during these steps may result in slight rotation or tilt of the lamella, leading to difficulties during the "thinning steps." Steps 8–12 in Table 1 correspond to Figures 3d to 3g, respectively. Figures 3d and 3e show the first transfer of the lamella to the grid with the AF stage set 90°, as we decided to perform back-side milling in this example. If the front-side milling would have been preferred, the AF stage would have been set to 0°. After the lamella has been released to the micro-manipulator, the AF stage is then rotated to a setting of 0° for back-side milling (90° in the case of front-side milling), in order for the lamella to be close to horizontal. The lamella is then reattached to the micro-manipulator and detached from the grid using the FIB, and the standard grid holder is exchanged for the homemade FIB holder (Fig. 1) by venting the chamber of the FIB workstation. These steps take 15 min of FIB time, plus the venting time of the main chamber.

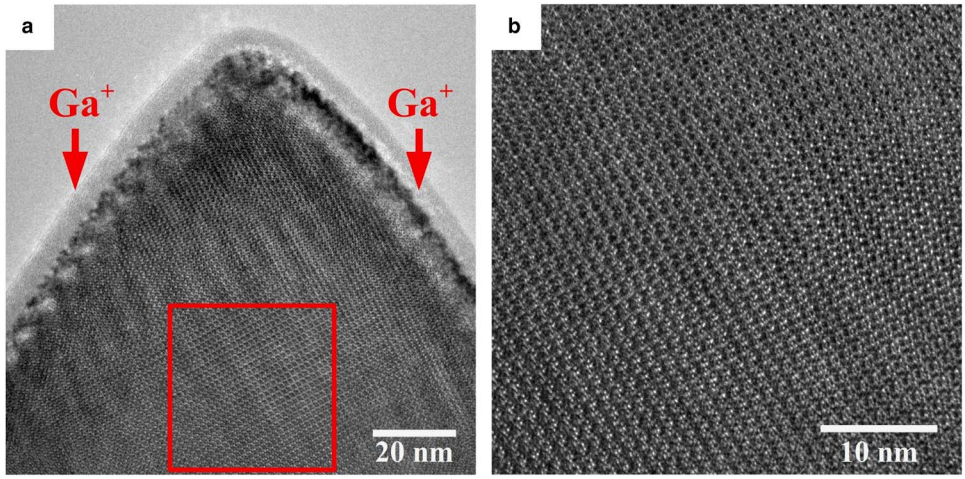

Figure 5. High-resolution transmission electron microscopic images of the complex metallic alloy specimen attached to a DENSsolutions double-tilt heater chip for annealing experiments. **a:** Lower side of the lamella in the back-side milling configuration [exposed to the focused ion beam (FIB) during the thinning procedure]. **b:** Magnified area shown by the red box in (**a**), ~50 nm from the specimen edge. The red arrows in (**a**) show the FIB milling direction.

Transfer of the Lamella to the Heater Chip

The next part of the procedure involves transfer of the thick lamella, which was previously rotated to a horizontal position, from the grid to the heater chip. The lamella should be placed as parallel as possible to the heater chip surface, in order to be able to take advantage of the full tilt range offered by the double-tilt heating holder (inset in Fig. 1). During the transfer steps, the lamella is in the horizontal position and may therefore be irradiated by the FIB if insufficient care is taken. In order to minimize damage due to irradiation, snapshots rather than continuous images are recorded when imaging with the FIB. The FIB energy is also switched to 5 keV in order to decrease the penetration depth of the Ga ions and to prevent contamination of the inner part of the lamella. Although the lamella should ideally be parallel to the heater chip surface, it can then only be thinned from one side, which is not desirable as both sides have to be cleaned. We found the optimal angle between the lamella and the heater chip to be ~13°. Figure 3h shows a lamella in its final position on the heater chip, still attached to the micro-manipulator, for which the stage tilt is set to 13°. Figure 3i shows the lamella attached to the heater chip at its lower surface using Pt deposition (marked by red arrows in Fig. 3i). The micro-manipulator tip is then cut free from the lamella (step 14 in Table 1).

Thinning Procedure

The FIB milling parameters, including the specimen thicknesses at which the accelerating voltage should be changed and the sample tilts used during milling, depend on the material system, and the values given here are optimal for preparing a CMA specimen to study dislocation propagation. In order to minimize Ga penetration into the lamella, the FIB was operated at 5 kV for all of the milling steps. The voltage was decreased progressively during the thinning procedure as the lamella became thinner, as described in steps 15–19 in Table 1. Each step was performed using FEI's RCS scanning pattern. Lower FIB energies than those given in Table 1 can be used after step 19 if the sample is particularly sensitive to Ga damage. The present specimen geometry allows a first check to be performed using a STEM detector inside the FIB system. Figures 4g to 4i show bright-field (BF), dark-field, and high-angle annular dark-field (HAADF) STEM images of the CMA lamella prepared in the present study.

BF and High-Resolution Transmission Electron Microscopy (HRTEM) Imaging

HRTEM images of the final TEM lamella on the heater chip are shown in Figure 5. Figure 5a shows the most unfavorable part of the lamella in terms of ion irradiation damage, i.e., the back-side surface of the lamella that was exposed to the FIB during the thinning steps in the back-side milling configuration without a protective Pt layer. The damaged upper-most part of the lamella comprises ~10 nm of amorphized material and a further ~10 nm damaged layer that is not fully amorphized. If required, the use of a lower FIB voltage than 5 kV during the final thinning steps could be used to reduce the thickness of these damaged layers (Schaffer et al., 2012).

More importantly, the thickness of the damaged layer in the region of primary interest on the lamella, i.e., on its lateral sides, is much thinner than the value of 20 nm mentioned above. In these regions, FIB damage is not caused by direct implantation of Ga ions at an angle of 90 ± 5° to the front side of the lamella, according to step 19 in Table 1 (as shown by the red arrows in Fig. 5a), but by ions that travel parallel to the lateral sides of the lamella. The penetration depth of these ions is expected to be approximately one order of magnitude lower when compared with that for 90° implantation (Orloff et al., 2003). Figure 5b shows an HRTEM image taken 50 nm

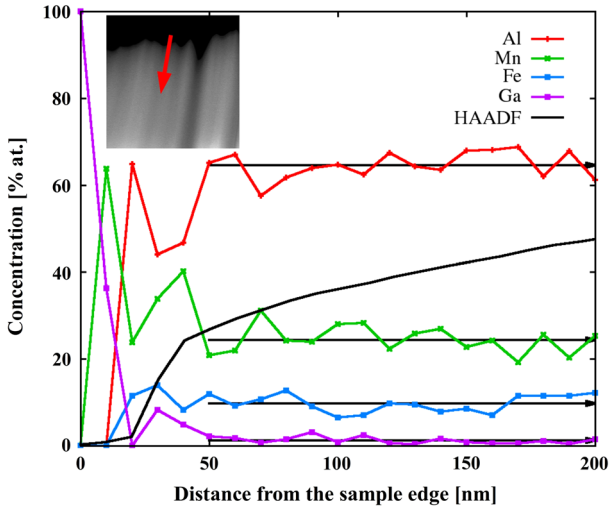

Figure 6. Energy-dispersive X-ray spectroscopy linescan recorded close to the specimen edge along the red arrow shown in the high-angle annular dark-field (HAADF) scanning transmission electron microscopic image (inset). The horizontal black lines show the average elemental concentration of each element 50 -200 nm from the specimen edge.

from the top edge of the lamella. Damage cannot be discerned in Figure 5b and the image quality can be compared with state-of-the-art HRTEM images of similar materials published elsewhere (Heggen et al., 2010, 2011). No significant specimen thickness variations at high magnification, which would result in strong lattice fringe contrast variations in a CMA material that has a large unit cell, are visible.

EDX Spectroscopy

In order to check for the presence of Ga due to FIB specimen preparation, EDX spectra were acquired from the upper-most part of the lamella obtained in the back-side milling configuration (close to the back-side surface). The inset to Figure 6 shows an HAADF STEM image recorded from this area of the specimen. Figure 6 shows Ga, Al, Mn, and Fe compositional profiles measured along the line marked by a red arrow in the HAADF STEM image. Within the first ~20 nm of the upper-most part of the lamella, the Ga concentration is significant, reaching a value of 100 at% at the specimen edge. At a distance of >50 nm from the specimen edge, the measured Ga concentration is below the detection limit of our EDX setup, while the concentration of elements in the CMA material is close to that reported previously, providing confidence in the EDX spectroscopy measurements, which were obtained using K edges and *k*-factors calculated using FEI's TIA software.

Conclusions

The complete preparation of TEM specimens for *in situ* TEM annealing experiments in a FIB workstation has been described. The final specimen quality is suitable for state-of-the-art TEM studies at elevated temperature. Similar procedures could be used to prepare TEM specimens for *in situ* straining and *in situ* electrical biasing experiments on MEMS-based devices.

Acknowledgments

The authors are grateful to Doris Meertens and Maximilian Kruth for their feedback when using the transfer procedure and Rolf Speen for designing the FIB holder. The authors would also like to acknowledge Dr. Michael Feuerbacher and Dr. Marc Heggen for providing the specimen used in the present study. The authors acknowledge financial support from the European Union under the Seventh Framework Programme under a contract for an Integrated Infrastructure Initiative. Reference 312483-ESTEEM2.

References

Balanetshyy, S., Meisterernst, G. & Feuerbacher, M. (2011). The Al-rich region of the Al-Mn-Ni alloy sytem. Part I: Ternary phases at the 750-950°C. *J Alloys Compd* **209**, 3787–3794.

Dunin-Borkowski, R.E., Newcomb, S.B., Kasama, T., McCartney, M.R., Weyland, M. & Midgley, P.A. (2005). Conventional and back-side focused ion beam milling for off-axis electron holography of electrostatic potentials in transistors. *Ultramicroscopy* **103**, 67–81.

FEI Company, xT (2003). *Nova NanoLab User's Manual* (1st ed.). Eindhoven: FEI Company, xT. pp. 5–57.

Field, R.D. & Papin, P.A. (2004). Location specific in situ TEM straining specimens made using FIB. *Ultramicroscopy* **102**, 23–26.

Figuerola, A., van Huis, M., Zanella, M., Genovese, A., Marras, S., Falqui, A., Zandbergen, H.W., Cingolani, R. & Manna, L. (2010). Epitaxial CdSe-Au nanocrystal heterostructures by thermal annealing. *Nano Lett* **10**, 3028–3036.

Giannuzzi, L.A., Drown, J.L., Brown, S.R., Irwin, R.B. & Stevie, F.A. (1997). Focused ion beam milling and micromanipulation lift-out for site specific cross-section TEM specimen preparation. *Mater Res Soc Symp Proc* **480**, 19–27.

Harlow, W., Ghassemi, H. & Taheri, M.L. (2014). In-situ TEM study of the corrosion behavior of Zry-4. *Microsc Microanal* **20**(Suppl 3), 1602–1603.

Heggen, M., Houben, L. & Feuerbacher, M. (2010). Plastic deformation mechanism in complex solids. *Nat Mater* **9**, 332–336.

Heggen, M., Houben, L. & Feuerbacher, M. (2011). Metadislocations in complex metallic alloys T-Al-Mn- (Pd, Fe). *Acta Mater* **59**, 4458–4466.

Jeangros, Q., Faes, A., Wagner, J.B., Hansen, T.W., Van Herle, J., Hessler-Wyser, A. & Dunin-Borkowski, R.E. (2010). In situ redox cycle of a nickel-YSZ fuel cell anode in an environmental transmission electron microscope. *Acta Mater* **58**, 4578–4589.

Kempshall, B.W., Schwarzx, B.W. & Giannuzzi, L. (2002). In situ FIB lift-out for site specific TEM specimen preparation of grain boundaries and interfaces. *Int Congress Electron Microsc Durban South Africa Proc* **1**, 249.

Langford, R.M., Huang, Y.Z., Lozano-Perez, S., Titchmarsh, J.M. & Petford-long, A.K. (2001). Preparation of site specific

transmission electron microscopy plan-view specimens using a focused ion beam system. *J Vacuum Sci Technol B* **19**, 755–758.

Langford, R.M. & Petford-Long, A.K. (2000). Preparation of transmission electron microscopy cross-section specimens using focused ion beam milling. *J Vacuum Sci Technol A* **19**, 2186–2193.

Legros, M., Dehm, G., Keller-Flaig, R.M., Arzt, E., Hemker, K.J. & Suresh, S. (2001). Dynamic observation of Al thin films plastically strained in a TEM. *Mater Sci Eng A* **463**, 309–310.

Longworth, H.P. & Thompson, C.V. (1991). Abnormal grain growth in aluminum alloy thin films. *J Appl Phys* **69**, 3929–3940.

Orloff, J., Utlaut, M. & Swanson, L. (2003). *High Resolution Focused Ion Beams: FIB and its Applications*, 1st ed. New York, NY: Kluwer Academic/Plenum Publishers.

Radulescu, F., McCarthy, J.M. & Stach, E. (2000). In situ annealing transmission electron microscopy study of Pd/Ge/Pd/GaAs interfacial reactions. *Mater Res Soc Symp Proc* **589**, 179–184.

Ramasse, Q., Anapolsky, A., Lazik, C., Jin, M., Armstrong, K. & Wang, D. (2009). Atomic scale observation and characterization of redox-induced interfacial layers in commercial Si thin film photovoltaics. *J Appl Phys* **105**, 033716.

Rogers, M., Kothleitner, G., Berendes, A., Bock, W. & Kolbesen, B.O. (2005). Focused ion beam preparation and EFTEM/EELS studies of vanadium nitride thin films. *Pract Metallography* **42**, 172–187.

Schaffer, M., Schaffer, B. & Ramasse, Q. (2012). Sample preparation for atomic-resolution STEM at low voltages by FIB. *Ultramicroscopy* **114**, 62–71.

van Huis, M.A., Kunneman, L.T., Overgaag, K., Xu, Q., Pandraud, G., Zandbergen, H.W. & Vanmaekelbergh, D.L. (2008). Low-temperature nanocrystal unification through rotations and relaxations probed by in situ transmission electron microscopy. *Nano Lett* **8**, 3959–3963.

van Huis, M.A., Young, N.P., Pandraud, G., Creemer, J.F., Vanmaekelbergh, D., Kirkland, A.I. & Zandbergen, H.W. (2009). Atomic imaging of phase transitions and morphology transformations in nanocrystals *Adv Mater* **21**, 4992–4995.

Venkatraman, R., Bravman, J.C., Nix, W.D., Davies, P.W., Flinn, P.A. & Fraser, D.B. (1990). Mechanical properties and microstructural characterization of AI-0.5%Cu thin films. *J Electron Mater* **19**, 1231–1237.

Xu, Q., Wu, M.Y., Schneider, G.F., Houben, L., Malladi, S.K., Dekker, C., Yucelen, E., Dunin-Borkowski, R.E. & Zandbergen, H.W. (2013). Controllable atomic scale patterning of freestanding monolayer graphene at elevated temperature. *ACS Nano* **7**, 1566–1572.

Zheng, P., Ruault, M.O., Denanot, M.F., Descouts, B. & Krauz, P. (1991). In situ thermal annealing of InP amorphous layer induced by Si^+ implantation. *J Appl Phys* **69**, 197–202.